Primljen / Received: 4.7.2025.
Ispravljen / Corrected: 1.10.2025.
Prihvaćen / Accepted: 16.10.2025.
Dostupno online / Available online: 10.3.2026.

Experimental investigation of the coordinated working performance of high-strength reinforcement and UHPC under varying parameters

Authors:

Shaofeng He, PhD. CE
Hebei University of Engineering, China
Faculty of Civil Engineering
The Key Laboratory of Urban Security and Disaster Engineering, Beijing University of Technology
heshaofeng@hebeu.edu.cn
Corresponding author

Linlin Tian, MSc. CE
CCCC Second Harbor Engineering Company Ltd., Wuhan, China
1059783771@qq.com

Meng Li, MCE
Shanghai University, China
Faculty of Mechanics and Engineering Sciences
li2211325308@126.com

Research Paper

Shaofeng He, Linlin Tian, Meng Li

Experimental investigation of the coordinated working performance of high-strength reinforcement and UHPC under varying parameters

The development of ultrahigh-performance concrete (UHPC) has prompted extensive research into the preparation and evaluation of UHPC performance. However, limited studies have explored the coordinated working performance of UHPC in conjunction with high-strength rebars within structural systems, particularly from a material-level perspective. This study investigated the relationship between the material mechanical properties and seismic performance of specimens under varying parameters by conducting cyclic tests on five reinforced UHPC columns with different configurations. The results demonstrated that high-strength rebars effectively constrains UHPC and enhances the bearing capacity of UHPC columns. In addition, incorporating a CFRP sheet or increasing the lateral confinement strength mitigated the expansion of UHPC in the core area and the concentration of local plastic damage. The UHPC and longitudinal reinforcement exhibited effective cooperative performance as the axial compression ratio increased.

Key words:
UHPC, high-strength reinforcement, coordinated working, seismic behaviour, coordinated work

Prethodno priopćenje

Shaofeng He, Linlin Tian, Meng Li

Eksperimentalno ispitivanje zajedničkog djelovanja armature visoke čvrstoće i UHPC-a pri različitim parametrima

Razvoj betona vrlo visokih uporabnih svojstava (eng. *Ultra-High Performance Concrete* - UHPC) potaknuo je opsežna istraživanja njegove pripreme i procjene ponašanja. Međutim, ograničen broj istraživanja bavio se usklađenim djelovanjem UHPC-a u kombinaciji s armaturom visoke čvrstoće u nosivim konstrukcijama, osobito s gledišta ponašanja materijala. U ovome istraživanju ispitivan je odnos između mehaničkih svojstava materijala i seizmičkog ponašanja ispitnih uzoraka pod različitim parametrima, provođenjem cikličkih ispitivanja na pet armiranih UHPC stupova različitih konfiguracija. Rezultati su pokazali da je armaturom visoke čvrstoće moguće učinkovito oviti UHPC te povećati nosivost UHPC stupova. Nadalje, ugradnja CFRP traka ili povećanje bočnog pritiska ovijanja smanjili su bočno širenje UHPC-a u središnjoj zoni i koncentraciju lokalnih plastičnih oštećenja. UHPC i uzdužna armatura pokazali su učinkovito zajedničko djelovanje s porastom bezdimenzijske tlačne sile.

Ključne riječi:
UHPC, armatura visoke čvrstoće, usklađeno djelovanje, seizmičko ponašanje, zajedničko djelovanje

1. Introduction

Ultrahigh-performance concrete (UHPC) meets the stringent strength and ductility requirements of modern concrete structures. In addition, its superior mechanical and durability characteristics significantly extend the service life of structural components. Owing to the incorporation of fibres, UHPC exhibits a pseudo-ductile tensile behaviour, forming multiple cracks instead of a singular crack [1]. The fibre-induced crack-arresting mechanism influences the failure mode of UHPC specimens, resulting in substantial increases in both cracking strength and ultimate strength [2-4]. Prior studies have demonstrated that UHPC can fully or partially replace conventional reinforcements in reinforced UHPC specimens [5-7] thereby improving the impact resistance, shear and flexure capacity, and seismic performance of reinforced UHPC (R-UHPC) specimens [8-17]. Lin et al. [18] observed that as the concrete strength increased, the stiffness and strength of test specimens deteriorated. Additionally, steel rebars in reinforced concrete specimens fractured under cyclic loads [19]. Therefore, the expansion of R-UHPC specimens and the collaborative performance of UHPC with steel bars require further investigation.

Enhancing the seismic performance of both structural components and the overall structure can be achieved by optimizing these materials. High-strength reinforcement is a viable option for enhancing the seismic behaviour of UHPC specimens, as it alters the failure mode and enhances both bearing capacity and ductility [20-23]. He et al. [24, 25] investigated five R-UHPC columns under reciprocating loads and demonstrated that high-strength steel reinforcement enhanced ductility, improved deformation recovery of R-UHPC columns, and exhibited string compatibility with UHPC. Bayrak et al. [26], Ousalem et al. [27] and Rautenber et al. [28] investigated high-strength concrete beams reinforced with high-strength steel and revealed that crack propagation and shear capacity degradation were delayed, achieving robust seismic performance.

In addition to experimental investigations, the finite element method was employed to investigate the performance of the UHPC specimens. Yin et al. [29] predicted the behaviour of R-UHPC specimens under static flexural loading utilising an implicit solver in LS-DYNA and a plasticity-based constitutive model for concrete. Mao et al. [30] calibrated the concrete model parameters and simulated the performance of R-UHPC specimens subjected to blast loading. Singh et al. [31] validated the behaviour of R-UHPC beams employing a modified concrete-damaged plasticity model. Aeimi et al. [32] applied the finite element method to assess the seismic performance of a UHPC pier and demonstrated that the tensile strength of the UHPC significantly influenced the post-peak performance of the model.

However, limited studies have explored the coordinated performance of UHPC and high-strength rebars, particularly from a material-level perspective within structural systems. Therefore, this study analysed the relationship between material mechanical behaviour and seismic performance of specimens under varying parameters by conducting cyclic tests on five reinforced UHPC columns with different configurations.

2. Experimental design

2.1. Experimental materials

1) Ultra-high performance concrete

The raw materials utilised to prepare UHPC were P·II52.5R Portland superfine cement, silica fume, fly ash, mineral powder, quartz sand, steel fibre, and water. The material distributions are listed in Table 1. Cubic test specimens with a side length of 150 mm were cured under identical conditions as the test columns and then tested. The average compressive strength f_c, was 122.5 MPa, and the average tensile strength f_t, was 5.93 MPa.

In Table 1, the cement, silica fume, fly ash, and mineral powder data are presented as mass ratios. The sum of the binder materials (cement, silica fume, and fly ash) is set to 1.0. The data for the steel fibres were expressed as a volume ratio, which is, the percentage of the volume of steel fibres in the total volume of concrete.

2) Carbon fibre-reinforced polymer (CFRP)

A unidirectionally braided CFRP sheet, illustrated in Figure 1, exhibited a tensile strength of 3602 MPa and an elastic modulus of 2.33×105 MPa. The CFRP sheet was bonded to the surface of the specimen via immersion in glue, forming a CFRP sheet surrounding the specimen. The bond strength between the CFRP sheet and concrete was 3.5 MPa.

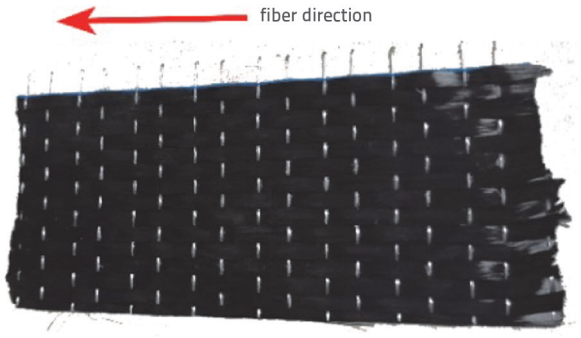

Figure 1. CFRP sheet

Table 1. Composition and mix proportion of UHPC

Superfine cement	Silica fume	Fly ash	Mineral powder	Water	Quartz sand	Volume fraction of steel fibre [%]
0.6	0.1	0.1	0.2	0.17	1.2	2.0

Table 2. Performance index of rebars

Symbol	Diameter [mm]	Maximum elongation	Yield strength [MPa]	Maximum strength [MPa]	Strain at the maximum load	Ratio of tensile strength to yield strength
Ø10	10	13 %	437	638	0.14	1.46
Ø16	16	17 %	436	599	0.16	1.37
Ø10	10	15 %	606	765	0.13	1.26
Ø16	16	18 %	551	712	0.17	1.29

Table 3. Design parameters of test columns

Specimen symbol	Longitudinal reinforcement	Reinforcement ratio ρ_s	Stirrup	Stirrup ratio ρ_{sv}	Test axial compressive ratio *n*	Thickness of CFRP sheet [mm]
NC80	10Ø16	3.22 %	Ø10/80	1.57 %	0.20	-
PNC80	10Ø16	3.22 %	Ø10/80	1.57 %	0.20	0.334
HC80	10Ø16	3.22 %	Ø10/80	1.57 %	0.20	-
HC100	10Ø16	3.22 %	Ø10/100	1.26 %	0.20	-
HC80h	10Ø16	3.22 %	Ø10/80	1.57 %	0.25	-

Note: H - the high-strength rebar, N - the normal-strength rebar, P - the carbon fibre-reinforced polymer (CFRP), C - the column, number in the specimen symbol - indicates the stirrup spacing, and h is the higher axial compression ratio.
ρ_s - represents the ratio of the cross-sectional area of the longitudinal reinforcement to the cross-sectional area of the column,
ρ_{sv} - represents the ratio of the cross-sectional area of the stirrups within each stirrup interval to the corresponding concrete area.

3) Reinforcement

Two types of reinforcements with different strengths were utilised in the test: HRB400 grade normal-strength rebar and HRB500 grade high-strength rebar. The longitudinal reinforcements and stirrups in the normal-strength rebar-reinforced UHPC column were Ø16 and Ø10, respectively, whereas those in the high-strength rebar-reinforced UHPC column were Ø16 and Ø10.

Three standard parts were reserved for each group of rebars for the material property test. The measured elastic modulus and yield strain of the rebar were 200 GPa and 0.002, respectively. The rebar strengths are listed in Table 2.

2.2. Specimen design

To investigate the influence of different confinement methods on the UHPC members, three confinement types were adopted: normal-strength rebar, high-strength rebar, and CFRP sheets. To examine the influence of confinement intensity, specimens with varying stirrup spacings were designed for comparison. Furthermore, to study the behaviour of UHPC under a high axial compression ratio and its effect on high-strength rebar confinement, specimens with different axial compression ratios were designed for comparative analysis. Therefore, one normal-strength rebar-reinforced UHPC short column, one CFRP sheet-restrained normal-strength rebar-reinforced UHPC column, and three high-strength rebar-reinforced UHPC columns were constructed in this study. The sectional dimensions of the columns were 250 mm × 250 mm, the shear–span ratio was 4.0, and the thickness of the concrete cover was 25 mm. The detailed design parameters of the specimens are listed in Table 3 and shown in Figure 2.

The CFRP sheet was fabricated by unidirectionally winding the CFRP fabric in a transverse fibre orientation. The CFRP fabric was bonded to the specimen and between the individual layers using an impregnation resin, which was air-dried to form a CFRP tube.

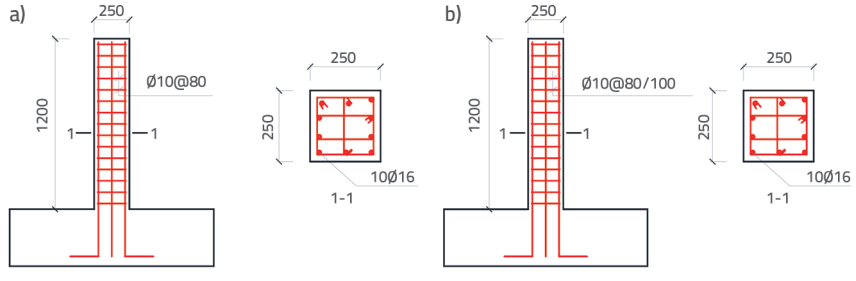

Figure 2. Details of specimen reinforcement: a) Specimens NC80 and PNC80; b) Specimens HC80, HC100, and HC80h

2.3. Test set-up, measurement, and loading protocol

2.3.1. Test set-up

Horizontal cyclic loading was applied to the specimens. An axial force was applied vertically on the top of the column, and the base was secured to the ground via anchor bolts. The setup is shown in Figure 3.

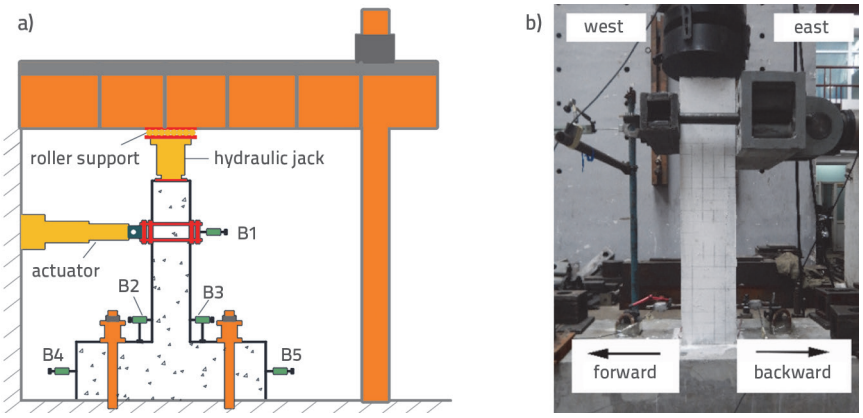

Figure 3. Loading equipment: a) Loading diagram; b) Test set-up

2.3.2. Loading protocol

Before testing commenced, an axial load was applied to the top of the specimen with an axial compression ratio of 0.2. For selected specimens, this axial load was maintained constant throughout the tests.

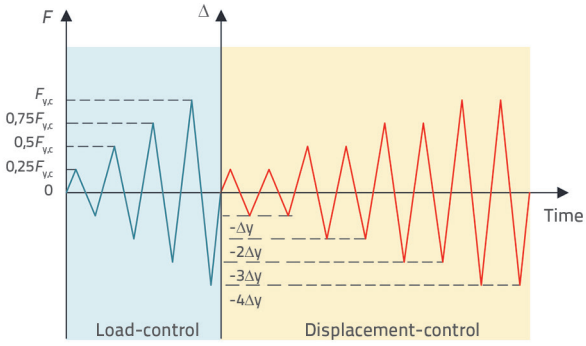

Figure 4. Loading protocol

Figure 4 shows the loading protocol. Pre-loading was performed before formal loading, and the pre-load was 25 % of the estimated cracking load. Subsequently, checks were conducted to ensure that the loading device was in full contact with the specimen and that the measuring instrument functioned normally. During the formal loading, a hybrid force-displacement control method was adopted. Prior to specimen yielding, when force-controlled loading was adopted, the strain growth was slow, enabling a more comprehensive observation of the strain development of the concrete and steel bars, loading 25 %, 50 %, 75 %, and 100 % of the estimated yield load with one load cycle at each stage. After the specimen yielded, concrete cracks no longer developed. After the specimen reached its yield point, cracks in the concrete nearly ceased to develop. At this juncture, the application of displacement loading can expedite the attenuation of the peak load. The displacement at each stage was Δ_y, $2\Delta_y$, $3\Delta_y$, and others (Δ_y is the yield displacement of the specimen). Each displacement stage was cycled twice, and the horizontal load was maintained for 5 min after each loading stage. The test was terminated when the horizontal load decreased to 85 % of the maximum load, indicating specimen failure.

2.3.3. Measurement

1) Displacement

Figure 3.a shows that five displacement sensors (B1–B5) were arranged in the test. B1 was positioned at the loading point to measure the applied load, while B2 and B3 were located 150 mm above the base to measure the rotation angle of the column. B4 and B5 were situated at the middle of the base to measure the horizontal slip during the test.

2) Reinforcement strain

Longitudinal steel strain gages R1–R8 were positioned at the four corner bars of the columns. Each corner bar had two strain gauges placed 50 and 150 mm above the top surface of the base, as shown in Figure 5.a.

The stirrup strain gauges were organised into three layers. The first stirrup above the top surface of the base constitutes the first layer, and the second and third stirrups form the second and third layers, respectively. The first layers of the stirrup strain gauges were L1-1 and L1-2, the second layers were L2-1 and L2-2, and the third layers were L3-1 and L3-2. Figure 5(b) shows the configuration of the stirrup strain gauges.

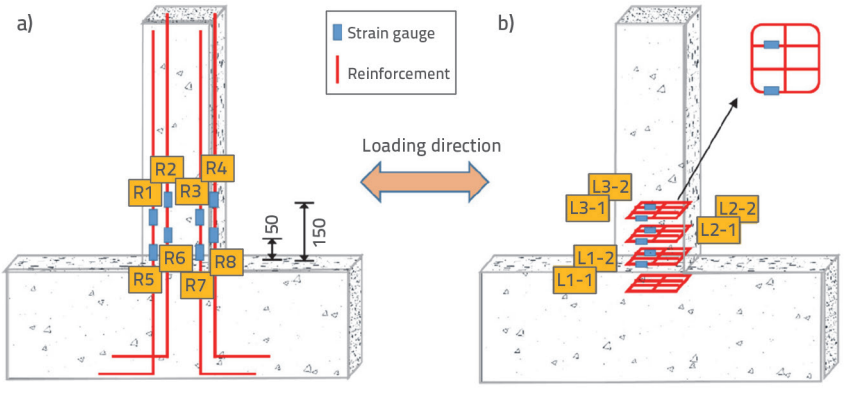

Figure 5. Locations of reinforcement strain gauges (unit: mm): a) Longitudinal steel strain gauges; b) Stirrup strain gauges

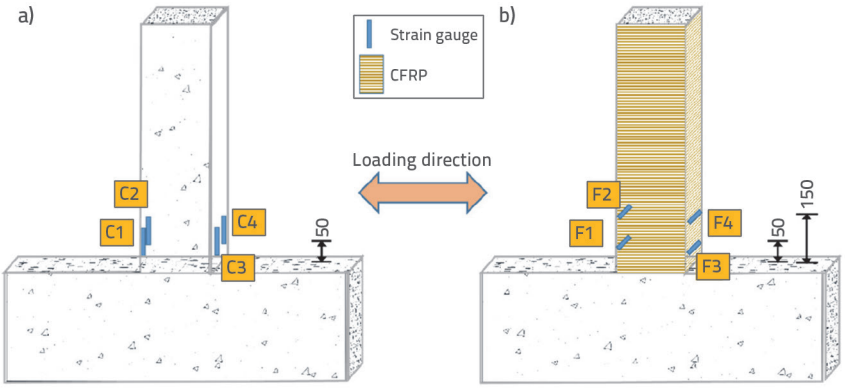

Figure 6. Locations of UHPC/CFRP strain gauges: a) Column without CFRP sheet; b) Column with CFRP sheet

3) UHPC/CFRP Strain

Four concrete strain gauges (C1–C4) were installed vertically 50 mm above the top surface of the base to monitor cracking in the concrete, as shown in Figure 6.a. Specimen PNC80 encased in a CFRP sheet did not allow direct measurement of the UHPC strain. The CFRP strains were measured at 50 mm and 150 mm above the top surface of the base. Figure 6.b illustrates the locations of the CFRP strain gauges (F1–F4), which also represent the operational state of the UHPC before the CFRP debonding occurred.

4) Other measurements

Horizontal loads were measured by a sensor attached to the actuator. All load, displacement, and strain measurements were collected employing a data acquisition instrument to achieve a one-to-one correspondence. During testing, the tension and compression cracks that emerged at each loading stage were marked on the specimens, and the lengths and maximum widths of the cracks were recorded.

3. Experimental results

Unless otherwise stated, the data and comparisons in the results and analysis represent the average values of both the forward and backward loading directions to reflect the actual structural behaviour.

Table 4. Characteristic load and displacement of R-UHPC columns

Specimen	Visible crack appeared		Longitudinal reinforcement yielded	Longitudinal reinforcement reached peak stress	
	Load [kN]	**Crack**	**Load** [kN]	**Load** [kN]	**Displacement** [mm]
NC80	160	West and north facades, transverse cracks	220	245.87	10.72
PNC80	-	-	250	250.78	15.72
HC80	200	East and north facades, transverse cracks	220	239.67	10.14
HC100	175	East facade, transverse cracks	220	219.46	13.33
HC80h	150	East and west facades, transverse cracks	180	247.94	10.21

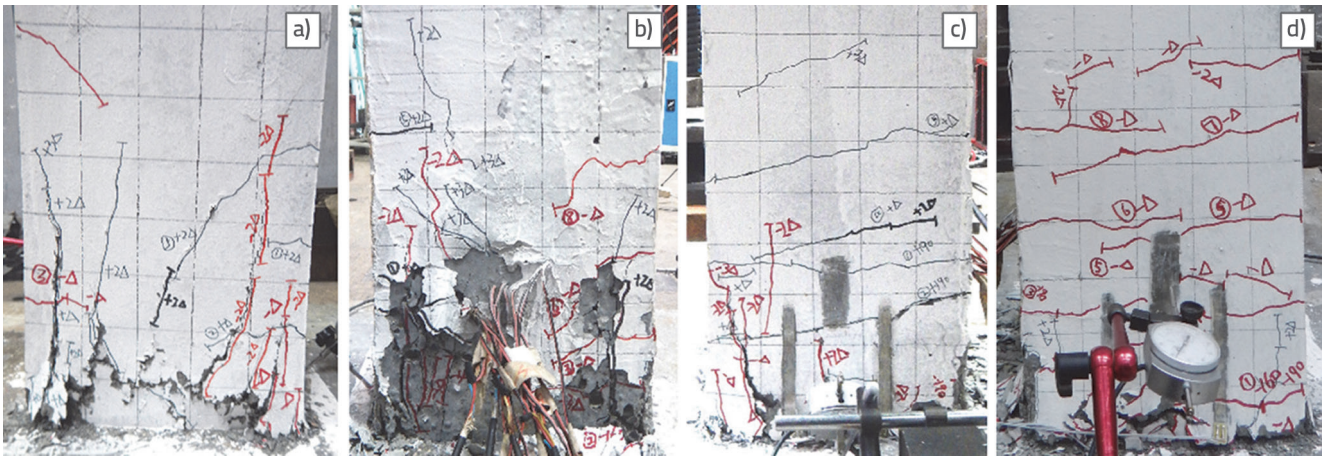

Figure 7. Failure mode of Specimen NC80: a) South (front); b) North (back); c) East; d) West

3.1. Test phenomenon

All specimens failed in the bending-shear mode. The failure process can be divided into three distinct stages: elastic deformation, elastoplastic deformation, and load degeneration. In the elastic stage, from the onset of loading until the appearance of the initial crack, the load-displacement relationship remained approximately linear and the specimen exhibited no residual deformation. In the elastoplastic stage, new cracks continued to form and develop stably, and the horizontal cracks at the bottom penetrated the surface of the cross-section; the longitudinal reinforcement yielded, and the load increased gradually with displacement; and the specimen displayed residual deformation after unloading. During the load degeneration stage, the longitudinal reinforcement reached its peak stress, and the load decreased with increasing displacement; the horizontal cracks at the base of the column developed into main cracks, and nearly no new cracks appeared on the surface of each specimen. The characteristic loads and displacements of each specimen are listed in Table 4.

Figure 8. Failure mode of Specimen PNC80: a) East; b) South

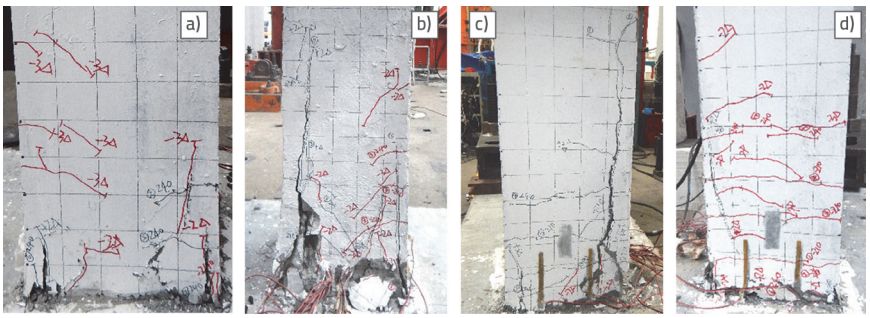

Figure 9. Failure mode of Specimen HC80: a) South (front); b) North (back); c) East; d) West

3.2. Characteristics of the hysteresis curves of the reinforced UHPC columns

The hysteresis curves of the reinforced UHPC columns are depicted in Figure 10. Figure 10 indicates that before the longitudinal reinforcement yielded, the load–displacement curves of the specimens consistently demonstrated linear elastic behaviour without plastic deformation. Upon yielding, the plastic deformation of the specimens increased and the hysteresis loop of the reinforced

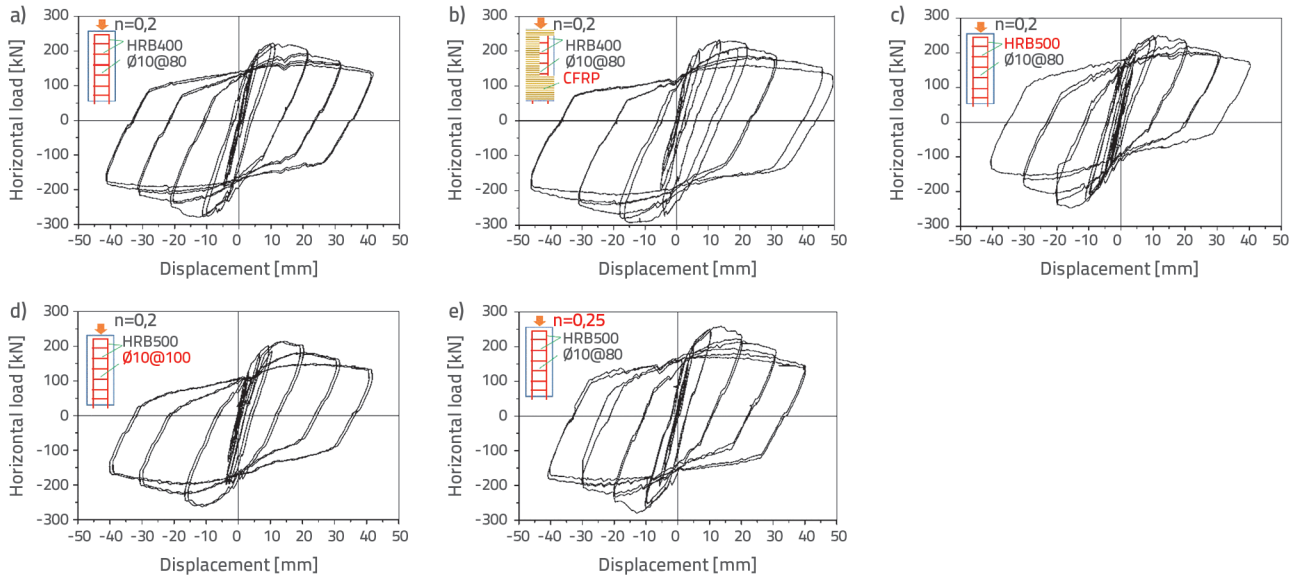

Figure 10. Hysteresis loops of the reinforced UHPC columns: a) Specimen NC80; b) Specimen PNC80; c) Specimen HC80; d) Specimen HC100; e) Specimen HC80h

UHPC column became full, presenting an ideal closed diamond shape without any significant pinching effect. Figure 11 shows a schematic comparison of the hysteresis curve shapes of ordinary reinforced concrete columns and reinforced UHPC columns.

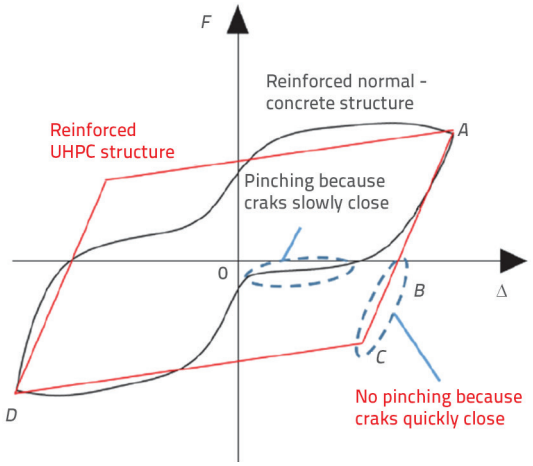

Figure 11. Comparison of hysteretic curve shapes

The force analysis of the characteristic points on the hysteretic curves is shown in Figure 12. When the specimens reached the maximum load (+F_{max}, point A), the tensile longitudinal ribs (A_s) in the tensile zone yielded, resulting in significant plastic deformation and maximum crack opening width. Upon unloading to zero (**F** = 0, point B), the specimens exhibited residual deformation, indicating that the bending crack was not completely closed at this point, and the bottom longitudinal bar (A_s) remained elongated, despite being compressed under the axial force. When a reverse load (F < 0, phase BC) was applied, the upper UHPC and steel bar (A'_s) shifted from compression to tension. The cracks in the lower UHPC rapidly closed, the pressure was shared with the steel bar (A'_s), and the curve did not exhibit pinching. With continuous reverse loading (F<0, phase CD), the tensile yield and UHPC cracks developed in the upper reinforcement (A_s), the stiffness of the specimens decreased, and the displacement increased substantially. As the crack width in the upper UHPC reached its maximum, damage accumulation reached a critical level, and the specimens attained the reverse maximum load (-F_{max}, point D). The skeleton curve of all specimens are shown in Figure 13.

The hysteresis curves of CFRP sheet-constrained specimens PNC80 and NC80 exhibited similar overall shapes. However, specimen PNC80 demonstrated a larger characteristic displacement; therefore, its total energy dissipation was greater than that of specimen NC80. Figure 10.b and 13.a indicate that CFRP sheet confinement can decelerate the bearing capacity attenuation of the reinforced UHPC, enhancing the ductility of the specimens.

Figure 10.c shows that the bearing capacity of specimen HC80 was lower than that of specimen NC80 during reverse loading owing to the influence of specimen defects. However, under forward loading, specimen HC80 exhibited higher load capacity owing to the enhanced strength of the longitudinal steel and stirrups. Compared with specimen NC80, the specimen HC80 exhibited smaller residual deformation during unloading, indicating stronger deformation recovery capability of the high-strength-reinforced UHPC columns.

Compared with specimen HC80, the bearing capacity of specimen HC100 decreased at a lower reinforcement ratio, and its residual deformation after unloading was more pronounced, indicating that UHPC columns under weak reinforcement experienced more extensive plastic deformation accumulation. The forward-loading skeleton curve in Figure 13.b shows that the attenuation rate of the bearing capacity of HC100 is comparable to that of HC80. Figure 10.e shows that compared with specimen HC80, the bearing capacity of specimen HC80h under a higher axial compression ratio was enhanced, and the residual deformation after unloading increased correspondingly. The bearing capacity degradation during the later stages of the test also increased.

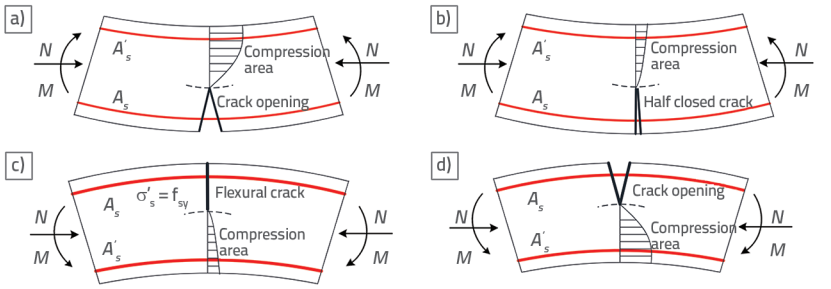

Figure 12. Stress analysis of the characteristic points of the hysteretic curves: a) point A: + F_{max}; b) point B: F = 0; c) point C: F < 0; d) point D: - F_{max}HC100 and HC80h

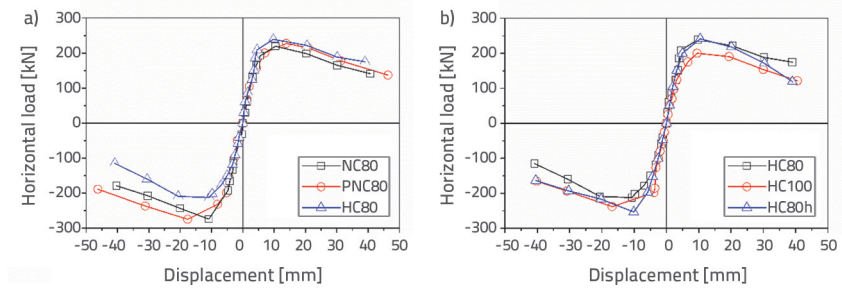

Figure 13. Skeleton curves of reinforced UHPC long columns: a) Specimens NC8, PNC80, and HC80; b) Specimens HC80, HC100, and HC80h

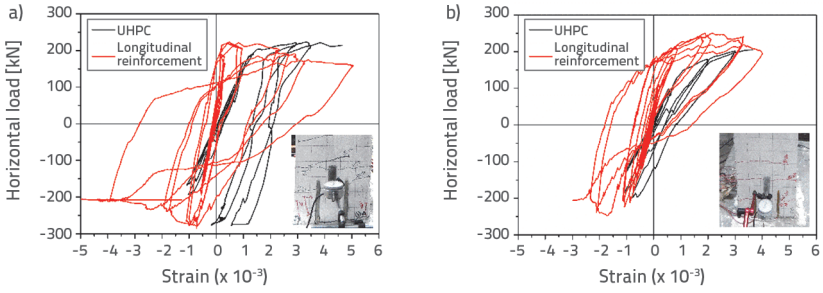

Figure 14. Strain-horizontal load curves of UHPC and longitudinal reinforcement on the same surface: a) Specimen NC80; b) Specimen HC80

4. Coordinated working performance of high-strength steel and uhpc under bending and shear failure

4.1. Effect of different reinforcement strengths

The strains of UHPC and longitudinal rebars on the same façade of specimens NC80 and HC80 were measured to evaluate the coordinated operational performance of normal- and high-strength steels combined with UHPC, as illustrated in Figure 14. This indicates that the development of the UHPC and longitudinal steel strains in the two specimens at the initial loading stage was similar, and the materials remained in the linear elastic stage. As the specimens underwent plastic deformation, material strains NC80 and HC80 exhibited different growth rates. The strain increments in the longitudinal steel and UHPC of NC80 were significantly greater than those of HC80 under the same load increment. Therefore, the UHPC specimens reinforced with high-strength steel bars demonstrated a greater resistance to cracking in the middle and late stages of the test. In addition, the coordinated performance of high-strength steel and UHPC was superior to that of normal-strength steel.

4.2. Effect of different confinement forms

When the crack depth was less than the thickness of the UHPC concrete cover, the longitudinal reinforcement strain steadily increased, whereas the UHPC stirrup strain in the core area increased marginally. As the crack depth exceeded the thickness of the UHPC cover, the crack propagated into the core area, significantly increasing the longitudinal steel strain (potentially turning off the strain gauge), and the stirrups began to exhibit plastic strain. Therefore, analysing the strains of the longitudinal steel and stirrups provides valuable insights into the cracking or expansion processes of UHPC within the protective and core layers.

A longitudinal steel strain comparison of specimens NC80, PNC80, and HC80 at different column heights is shown in Figure 15 for three different confinement forms: normal-strength steel rebars, CFRP sheets, and high-strength rebars. This comparison reveals that the increase in the longitudinal reinforcement strain in specimen HC80 is lower than that in NC80, indicating that the configuration of the high-strength steel bars can transmit stress more effectively on both sides of the crack, thereby slowing the development of UHPC cracks. Compared with specimens NC80 and PNC80, the longitudinal reinforcement strain in specimen HC80 at a column height of 50 mm increased significantly in the later stage of the test, whereas the strain at a column height of 150 mm increased only marginally. This is attributed to the primary plastic deformation of the specimen concentrated at the edge of the CFRP sheet at the column base, whereas crack development in the CFRP sheet at other positions was effectively inhibited.

The stirrup strains of specimens NC80, PNC80, and HC80 at different column heights (50 and 210 mm) under three confinement conditions (normal-strength rebar, CFRP sheet, and high-strength rebar) are shown in Figure 16.

Figure 16(a) shows that the stirrup strain in specimen NC80 significantly increased at column heights of 50 and 210 mm during the later stages of the test, indicating a suboptimal restraining effect on the UHPC within the core area. As CFRP sheet confinement was introduced, the stirrup strain amplitude in specimen PNC80 at the bottom of the column (height of 50 mm) decreased substantially, and the stirrups demonstrated some capacity for deformation recovery. At a column height of 210 mm, the stirrup strain in PNC80 decreased marginally, and the CFRP sheet effectively mitigated the expansion of UHPC in the core area. With an elevated strength grade in specimen HC80, the increase in the stirrup strain at column heights of 50 and 210

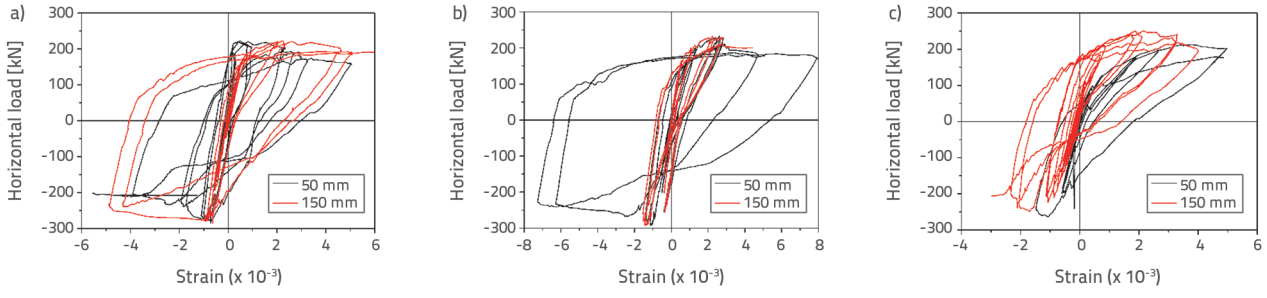

Figure 15. Strain comparison of longitudinal steel under different column heights: a) Specimen NC80; b) Specimen PNC80; c) Specimen HC80

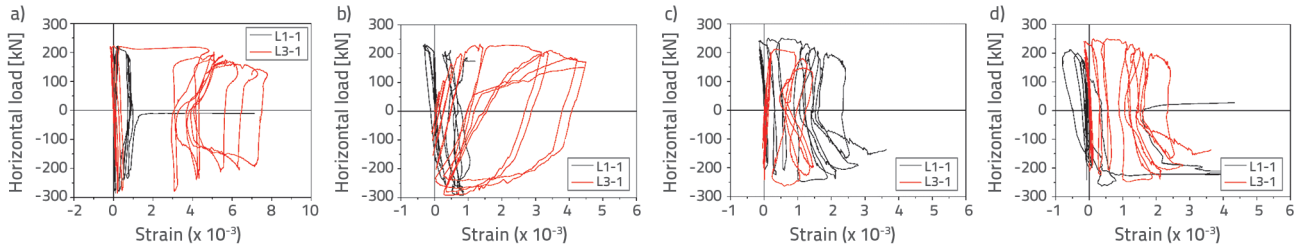

Figure 16. Strain comparison of stirrup under different column heights: a) Specimen NC80; b) Specimen PNC80; c) Specimen HC80; d) Specimen HC100

mm was reduced, validating that the high-strength reinforcement provided a more effective restraint on the UHPC in the core area. The effects of the CFRP sheet and rebar strength grade on the working mechanism of the reinforced UHPC columns under bending and shear failure are shown in Figure 17. The symbols ε_{NC80}, ε_{PNC80}, and ε_{HC80} represent the stirrup strains of specimens NC80, PNC80, and HC80, respectively. Incorporating a CFRP sheet can marginally constrain the UHPC expansion in the core area; however, it leads to a concentration of plastic damage at the edge of the CFRP sheet. Enhancing the strength grade of the rebars transmits stress across the cross-sections more effectively, thereby limiting the expansion and deformation of UHPC in the core area and preventing the concentration of local plastic damage.

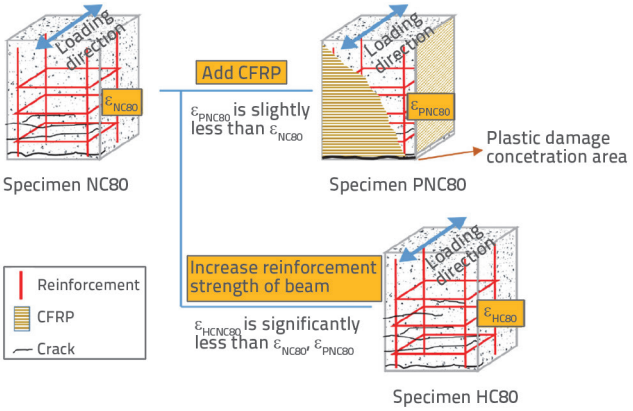

Figure 17. Influence of different confinement forms on the working mechanism

4.3. Effect of different confinement strengths

The lateral confinement strength σ_1 of the stirrups is defined as shown in Equation (1):

$$\sigma_1 = \frac{A_{sv}}{sb_{cor}} f_{yv} \tag{1}$$

where f_{yv} is the measured yield strength of the stirrups; A_{sv} is the sum of the cross-sectional areas of each leg of the stirrups in the loading direction. If the number of stirrup legs differs in the two principal directions of the cross-section, a smaller value of A_{sv} from the two directions is adopted; s is the stirrup spacing; b_{cor} is the width of the stirrups on the periphery of the UHPC in the core area in the loading direction.

The stirrups of specimens NC80, HC80, and HC100 with varying strengths and spacing provided different lateral confinement strengths for UHPC in the core area. Based on Equation (1), the calculated values of the lateral stress, σ_1, for the three specimens were 7.46, 9.40, and 7.52, respectively. The development of the stirrup strain in specimens NC80, HC80, and HC100 corresponded to the applied horizontal load, as illustrated in Figs. 16.a, 16.b and 16.d. In addition, the degree of expansion of UHPC in the core area at the bottom exceeded that in the upper part of the column, and the expansion amplitude of UHPC in the core area reduced as σ_1 increased.

The stirrup strain increment $\Delta\varepsilon_{sv}$ and amplitude of the bearing capacity degradation D_F were defined using Equations (2) and (3) to assess the extent to which the UHPC in the core area expanded under various confinement intensities after the peak load.

$$\Delta\varepsilon_{sv} = \varepsilon_{sv} - \varepsilon_{sv,p} \tag{2}$$

$$D_F = (F_p - F)/F_p \tag{3}$$

where ε_{sv} and $\varepsilon_{sv,p}$ are the strains corresponding to the real-time strain and peak load of the stirrups, respectively; F and F_p are the real-time and peak loads of the specimen, respectively.

Owing to the failure of some reinforcement strain gauges during the loading process, data from strain gauge L3-1 were selected exclusively, and the stirrup strain increment after the peak load under different bearing degradation amplitudes was computed, as shown in Figure 18. As the horizontal load decreased, the stress within the stirrups continued to increase, indicating the ongoing expansion of UHPC in the core area. The slope of the curve indicates that the rate of UHPC expansion in the core area declines as σ_1 increases.

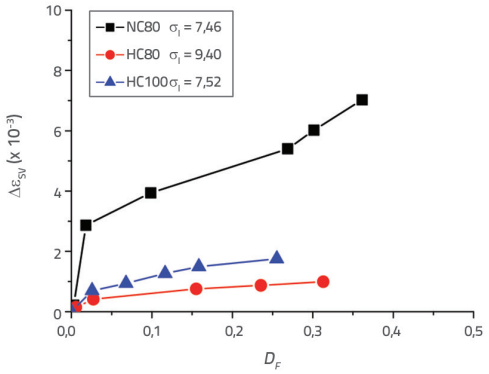

Figure 18. Strain increment of stirrups under different load degeneration

4.4. Effect of a high axial compression ratio

At high axial compression ratios, transverse cracks in the UHPC column were suppressed at the onset of the test, whereas the formation of vertical microcracks was promoted. This behaviour facilitates debonding between the longitudinal reinforcement and UHPC. Therefore, the degree of debonding of the longitudinal bars was assessed by comparing the strain of the longitudinal bars with that of UHPC at the same vertical position using the following procedure:

- measure the strain of longitudinal reinforcement and UHPC at the same height
- convert the UHPC strain to align with the cross-sectional height of the longitudinal reinforcement strain because the strain gauges of concrete and reinforcement are not installed at the same height, as depicted in Figure 5.a and Figure 6.a
- compute the ratio of UHPC strain to longitudinal reinforcement strain ($\varepsilon_c/\varepsilon_s$) as the horizontal coordinate, and plot the horizontal load-$\varepsilon_c/\varepsilon_s$ diagram, as shown in Figure 19.

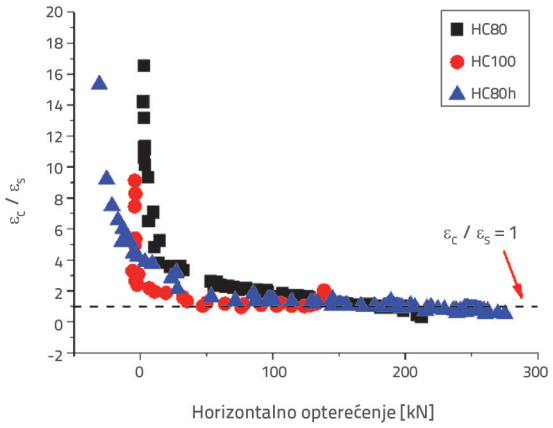

Figure 19. Relationship between horizontal load and $\varepsilon_c/\varepsilon_s$

When no slip occurs between UHPC and steel rebars, the materials act in full coordination; therefore, $\varepsilon_c/\varepsilon_s$ =1. Figure 19 indicates that UHPC predominantly provides the bending resistance of the specimen, and the longitudinal reinforcement strain is minimal, resulting in a higher $\varepsilon_c/\varepsilon_s$. As microcracks developed, the contribution of longitudinal reinforcement to bending resistance increased, and $\varepsilon_c/\varepsilon_s$ gradually approached 1. Compared with specimen HC80, specimen HC80h exhibited relatively stable $\varepsilon_c/\varepsilon_s$ as the axial compression ratio increased, indicating that the UHPC and longitudinal reinforcement maintained effective coordinated performance under high axial compression ratios. Conversely, in specimen HC100, as stirrup spacing reduced, the$\varepsilon_c/\varepsilon_s$ ration increased in the later loading stages, indicating that UHPC strain increased more rapidly than that of the reinforcement, reflecting a marginal decline in their coordinated performance.

5. Conclusion

This study analysed the relationship between the material mechanical behaviour and seismic performance of specimens under varying parameters by conducting cyclic tests on five reinforced UHPC columns with different configurations. The primary conclusions are as follows:

- The failure process of the reinforced UHPC columns can be categorised into three stages: quasi-elastic deformation, elastoplastic deformation, and load degeneration. The UHPC did not collapse throughout the process and the hysteresis loop was complete, exhibiting a relatively ideal closed diamond shape without significant pinching.
- The high-strength rebars provided effective confinement for the UHPC, enhancing the load-bearing capacity of the columns. Compared with columns utilising normal-strength rebars, those reinforced with high-strength rebars demonstrated less residual deformation in the loading stage, indicating a superior ability to recover from deformation. Specimens with high-strength rebars also exhibited increased resistance to cracking in the middle and late stages of testing, and their performance in coordination with the UHPC surpassed that of their normal-strength counterparts.
- Under bending and shear failure, the addition of CFRP sheets limited the expansion of the UHPC in the core area; however, this also resulted in a concentration of plastic damage at the edges of the CFRP sheet. Improving the reinforcement strength grade enhances the stress transmission across the cross-sections, controls the expansion and deformation of UHPC in the core area, and prevents localised plastic damage.
- The effect of multiple confinement intensities on UHPC in the core area was quantitatively assessed by defining the lateral confinement strength σ_1. As the load degenerated, the stress in the stirrups increased, indicating continuous expansion of the UHPC in the core area; however, the expansion rate decreased as σ_1 increased.
- As the axial compression ratio increased, the strain ratio between UHPC and longitudinal reinforcement, $\varepsilon_c/\varepsilon_s$, remained relatively constant, indicating that UHPC and longitudinal reinforcement exhibits effective cooperative performance. When the stirrup spacing was reduced, $\varepsilon_c/\varepsilon_s$ increased in the late loading stage, indicating that the strain in UHPC increases more rapidly than that in the longitudinal reinforcement, thereby marginally reducing their coordinated performance.

Acknowledgement

This work was supported by the Hebei University of Engineering (Grant No. SJ2401002115).

REFERENCES

[1] Leung, C.K.Y.: Design criteria for pseudo-ductile fiber-reinforced composites, Journal of Engineering Mechnics, 122 (1996), pp. 10-18.

[2] Mansur, M.A., Ong, K.C.G., Paramasivam, P.: Shear strength of fibrous concrete beams without stirrups, Journal of Structural Engineering, 112 (1986), pp. 2066-2079.

[3] Narayanan, R., Darwish, I.Y.S.: Use of the steel fibers as shear reinforcement, ACI Structural Journal, 84 (1987), pp. 216-227.

[4] Wang, Q., Bao, X., Yang, J., Xu, G., Zhang, M.: Investigation of ultrahigh-performance concrete fracture characteristics with different steel fiber fractions based on acoustic emission, Journal of Materials in Civil Engineering, 35 (2023) 12, pp. 04023437.

[5] Li, L.Z., Yang, B., Yu, K.Q., Yu, J.T., Lu, Z.D.: Reinforced high-strength engineered cementitious composite (ECC) columns under eccentric compression: Experimental and theoretical model, Engineering Structures, 198 (2019), pp. 109541.

[6] Qudah, S., Maalej, M.: Application of engineered cementious composites (ECC) in interior beam-column connections for enhanced seismic resistance, Engineering Structures, 69 (2014), pp. 235-245.

[7] Xu, L., Pan, J.L., Chen, J.H.: Mechanical behavior of ECC and ECC/RC composite columns under reversed cyclic loading, Journal of Materials in Civil Engineering, 29 (2017), pp. 04017097.

[8] Li, B., Lam, E.S., Wu, B., Wang, Y.Y.: Experimental investigation on reinforced concrete interior beam-column joints rehabilitated by ferrocement jackets, Engineering Structures, 56 (2013), pp. 897-909.

[9] Abbas, A.A., Mohsin, S.M.S., Cotsovos, D.M.: Seismic response of steel fibre reinforced concrete beam-column joints, Engineering Structures, 59 (2014), pp. 261-283.

[10] Aviram, A., Stojadinovic, B., Parra-Montesinos, G.J.: High-performance fiber-reinforced concrete bridge columns under bidirectional cyclic loading, ACI Structural Journal, 111 (2014) 2, pp. 303-312.

[11] Hu, R., Fang, Z., Benmokrane, B., Fang, W.: Cyclic behaviour of UHPC columns with hybrid CFRP/Steel reinforcement bars, Engineering Structures, 238 (2021), pp. 112245.

[12] Nadir, W., Kadhim, M.A., Jawdhari, A., Jawdhari, A., Fam, A., Majdi, A.: RC beams strengthened in shear with FRP-Reinforced UHPC overlay: An experimental and numerical study, Structures, 53 (2023), pp. 693-715.

[13] Wei, J., Li, J., Liu, Z., Wu, C., Liu, J.: Behaviour of hybrid polypropylene and steel fibre reinforced ultra-high performance concrete beams against single and repeated impact loading, Structures, 55 (2023), pp. 324-337.

[14] Chen, D., El-Hacha, R.: Flexural behaviour of hybrid FRP-UHPC girders under static loading, Proceedings of 8th International Conference on Short and Medium Span Bridge Niagara Falls, Canada, 2010.

[15] Zhu, J., Guo, X., Kang, J., Duan, M., Wang, Y.: Experimental investigation of flexural behavior of steel-UHPC composite beam with waffle-slab system, Journal of Bridge Engineering, 26 (2021) 4, Paper 04021011.

[16] Fu, T., Wang, K., Zhu, Z., et al.: Seismic performance of prefabricated square hollow section piers strengthened by jacketing using UHPC and high-strength steel, Structures, 47 (2023), pp. 449-465.

[17] Fang, S.: Bearing capacity of UHPC-filled circular steel tube short column under axial compression, GRAĐEVINAR, 77 (2025) 7, pp. 687-697, https://doi.org/10.14256/JCE.4173.2024

[18] Lin, H.B., Wang, Q.F.: Seismic behavior on HRB400 high-strength reinforced concrete columns, Journal Building Structures, S1 (2018), pp. 36-41, (in Chinese)

[19] Hung, C.C., Yen, W.M., Yu, K.H.: Vulnerability and improvement of reinforced ECC flexural members under displacement reversals: Experimental investigation and computational analysis, Construction and Building Materials, 107 (2017), pp. 287-298.

[20] Hassan, T.K., Seliem, H.M., Dwairi, H., Rizkalla, S.H., Zia, P.: Shear behavior of large concrete beams reinforced with high-strength steel, ACI Structural Journal, 105 (2008) 2, pp. 173-179, https://doi.org/10.14359/19732

[21] Yan, C., Jia, J., Zhang, J.: Seismic behavior of steel reinforced ultra-high strength concrete column and reinforced concrete beam connection, Transactions of Tianjin University, 16 (2010) 4, pp. 309-316.

[22] Wang, T.C., Liu, X., Zhao, H.L.: Seismic performance of cross-shaped columns with 500 MPa grade reinforcing steel bars, Tehnicki Vjesnik., 22 (2015) 3, pp. 629-636.

[23] Wang, T., Liu, X., Zhao, H.: Experimental research on seismic behavior of+-shaped columns reinforced with high-strength steel bars under cyclic loading, KSCE Journal of Civil Engineering, 19 (2015) 4, pp. 982-993.

[24] He, S.F., Deng, Z.C.: Seismic behaviour of ultra-high performance concrete short columns confined with high-strength reinforcement, KSCE Journal of Civil Engineering, 23 (2019), pp. 5183-5193, https://doi.org/10.1007/s12205-019-0915-3

[25] He, S.F., Deng, Z.C., Yao, J.S.: Seismic behavior of ultra-high performance concrete long columns reinforced with high-strength steel, KSCE Journal of Civil Engineering, 32 (2020), pp. 101740.

[26] Bayrak, O., Sheikh, S.A.: Confinement reinforcement design considerations for ductile HSC columns, Journal of Structural Engineering, 124 (1998) 9, pp. 999-1010.

[27] Ousalem, H., Takatsu, H., Ishikawa, Y., Kimura, H.: Use of high-strength bars for the seismic performance of high-strength concrete columns, Journal of Advanced Concrete Technology, 7 (2009) 1, pp. 123-134.

[28] Rautenberg, J.M., Pujol, S., Tavallali, H., Lepage, A.: Drift capacity of concrete columns reinforced with high-strength steel, ACI Structural Journal, 110 (2013) 2, pp. 307.

[29] Yin, H., Shirai, K., Teo, W.: Finite element modelling to predict the flexural behavior of ultra-high performance concrete members, Engineering Structures, 183 (2019), pp. 741-755.

[30] Mao, L., Barnett, S., Begg, D., Schleyer, G., Wight, G.: Numerical simulation of ultra-high performance fibre reinforced concrete panel subjected to blast loading, International Journal of Impact Engineering, 64 (2015), pp. 91-100.

[31] Singh, M., Sheikh, A.H., Mohamed Ali, M.S., Visintin, P., Griffith, M.C.: Experimental and numerical study of the flexural behaviour of ultra-high performance fibre reinforced concrete beams, Construction and Building Materials, 138 (2017), pp. 12-25.

[32] Naeimi, N., Moustafa, M.A.: Numerical modeling and design sensitivity of structural and seismic behavior of UHPC bridge piers, Engineering Structures, 219 (2020), pp. 110792.